Microchemical Journal xxx (2018) xxx-xxx

Contents lists available at ScienceDirect

Microchemical Journal

journal homepage: www.elsevier.com

Modern acrylic paints probed by optical coherence tomography and infrared reflectography

J. Striova[a,*], A. Dal Fovo[a], V. Fontani[b], M. Barucci[a], E. Pampaloni[a], M. Raffaelli[a], R. Fontana[a]

[a] INO-CNR, Sezione di Firenze, Largo Enrico Fermi 6, 50125 Firenze, Italy
[b] Università degli Studi di Firenze, Via della Lastruccia 3, 50019 Sesto Fiorentino (FI), Italy

ARTICLE INFO

Article history:
Received 24 July 2017
Received in revised form 6 December 2017
Accepted 29 December 2017
Available online xxx

Keywords:
Oct
Acrylic paints
Phthalocyanine
Non-invasive stratigraphy
Underdrawing visualization
Infrared imaging

ABSTRACT

Contemporary art is particularly delicate as the synthetic materials used for their realization are of poorer quality and durability than the traditional materials. It follows that the contemporary artworks often require imminent restorations as well as in-depth analytical studies of the constituting materials. The non-invasiveness of the scientific methods is a key issue in the diagnostics of contemporary art because it minimizes the need of sampling. In this respect, the potential of Optical Coherence Tomography (OCT) imaging to probe the internal structure of the commercial acrylic paint layers, as a function of their thickness, was investigated and compared with that of the near infrared (NIR) reflectography. In support of these measurements, micro-profilometry, an interferometric technique with micrometric depth resolution, was used to measure the paint layer thicknesses. We show that for some painted materials there is a limited possibility to visualize the underdrawings, when investigated by both OCT and NIR reflectography. This is owed to either the absorption of the illumination wavelength by the paint layer (Cobalt-based paints) or the multiple photon scattering effect (presence of TiO_2).

1. Introduction

The quest for non-invasive analyses is a key issue in the diagnostics of cultural heritage. Optical Coherence Tomography (OCT) is a non-invasive interferometric method employed for the non-contact imaging of the 3D subsurface internal microstructure of semi-transparent or transparent materials. It allows for obtaining high resolution cross-sectional tomograms of samples which moderately scatter and/or absorb the probing light. Huang et al. [1] introduced the OCT technique in the 1990s and since then it has been mainly used in ophthalmology for imaging human retinas in vivo through the iris of the eye and other biological tissues [2–4]. In the recent years, OCT technique has also been employed for non-medical purposes such as in studies of artworks [5–10]. The tomography of the object is generated by the interference between the reference and the reflected (or scattered) beam. The radiation impinging on the sample is backscattered from different depth interfaces and optically interferes whenever it overlaps, within the radiation coherence time, with a delayed reference field. Fundamental parameters of tomograms are the axial (depth, along the optical beam, z-axis) and transversal resolution (plane perpendicular to the beam, x-y axes). The source coherence length limits its depth resolution, whereas the focal spot size within the sample states the resolution transverse to the optical axis. Depth resolution improves as a function of the bandwidth of the illumination source and diminishes as its wavelength squared [11]. The information about the physical make-up of the examined artefact can be obtained provided the semi/transparency of probed layers. Most varnishes are detectable by OCT using infrared light. In fact, OCT proved to be a powerful tool in varnish drying studies [12], monitoring of laser ablation [13,14], in depth localization of varnish deterioration [15], varnish thinning [16,17]. On the other hand, only few studies deal with the transparency of pigments [18–21]. In fact, one major limitation of OCT imaging is the achievable probing depth through highly turbid paints. Szkulmowska et al. [19] described the 823 and 1550 nm OCT examination of different paints, highlighting that the longer wavelengths enable deeper penetration of the sample. However, the survey is rather qualitative not specifying the paint thicknesses, whose structure can be visualized in OCT tomogram. Liang et al. [18] found a clear correspondence between the pigment composition and the particle size, pointing out a considerable advantage in using higher wavelengths, especially when a fine grain material composes the analysed object. Liang's research team has demonstrated that the optimal spectral window for a deeper OCT analysis is around 2200 nm, due to the maximum transparency of most of the pigments. They have also developed several prototypes in the 2 μm spectral region, demonstrating the increase in the probing depth, however at cost of loss in axial resolution [22–24]. Our study aims at covering the information gap on the optical behaviour of paint materials, especially of contemporary pigments and dyes. Our previous study pointed to the 1550 nm OCT potential to investigate pthalocyanine paints [25]. In this respect, we designed an experiment involving different contemporary blue paint layers and examined them as a function of their thickness to demonstrate the limits and potentiality of OCT imaging in visualizing the subsurface microstructure.

* Corresponding author.
Email address: jstriova@gmail.com (J. Striova)

https://doi.org/10.1016/j.microc.2017.12.027
0026-265/

2. Materials and methods

2.1. Materials

The samples, simulating panel paintings, consist of a wooden support (30 cm in length and 3 cm in width) coated with four layers of preparatory ground (acrylic ground, Zecchi, no. 3030/750). Five different underdrawings a) Iron gall ink, Zecchi, art 5050/1; b) Charcoal, Nitram; c) Pb/Sn metal point, Zecchi; d) Sepia, Contè a Paris, France 1355 and e) Sanguine, Contè a Paris, France 610, were sketched on the ground in a scheme specified in Fig. 1 left. Blue paints (Extrafine acrylic colors Brera Acrylics, Maimeri industry) were then applied, in three thickness ranges (I-III), to cover a 2.5 × 3 cm area for each of the eight different paints. Thicknesses I, II and III – i.e. around 100, 200 and 300 μm, respectively- were obtained by applying respectively 30, 60 and 90 brushstrokes to the designated area (Fig. 1 right). The criterion to set the first thickness (30 brushstrokes) was the amount of the paint sufficient to guarantee the coverage of the underdrawing traits.

The compositional and commercial specifics of examined paints (Fig. 2) are described in Table 1, classified according to the pigment composition into 1) inorganics, 2) organics, 3) and mixtures.

The paints were checked for their elemental and molecular composition by PIXE and Raman spectroscopy; the detailed description of the results is beyond the scope of this article.

2.2. Methods

2.2.1. Microprofilometry

To determine the thickness of prepared paint layers, the specimens were investigated with a laser scanning microprofilometer, through a custom-made device developed by INO-CNR. The instrument includes a commercial conoscopic probe (composed of a birefringent crystal sandwiched between two circular polarizers) mounted on two motorized high-precision linear stages for horizontal and vertical movements. A laser diode emits a coherent monochromatic light beam ($\lambda = 655$ nm) on the sample surface, through the probe equipped with a 50 mm lens, which sets a stand-off distance of 4 cm with 8 mm dynamic range, 1 μm axial and 20 μm lateral resolution. For each sample, two measurements at t_0 (wooden supports with ground layer) and t_1 (wooden supports with ground and painted layers) with a sampling step of 50 μm were performed. For the positioning of the sample, we used a special custom-made holder that minimizes the deviations caused by repositioning. The support was removed from the holder for the paint application and then repositioned. A perfect alignment of the two meshes is not an easy task. In order to make the latter operation as precise as possible, we realized a series of incisions of different shape in the scotch tape used for delimitation of the paints, which were taken as reference markers for the alignment. The subtraction of height (z) values is performed in Matlab environment where operations as translation and rotation on the (x,y,z) maps are applied when necessary. The estimated error in the alignment procedure of the two meshes is about 25 μm (half the sampling step). The measured height values (at t_1 and t_0) were sub-

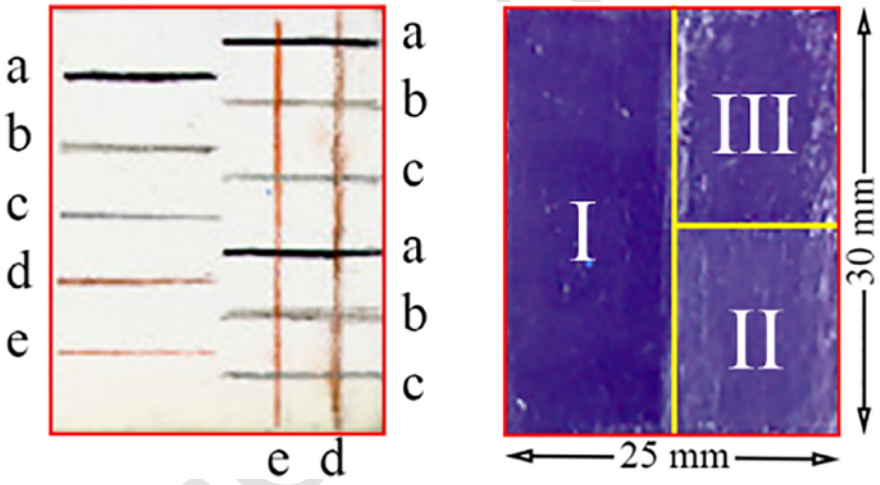

Fig. 1. Specimen: underdrawing pattern on ground (left); paint application scheme of three thickness ranges (right).

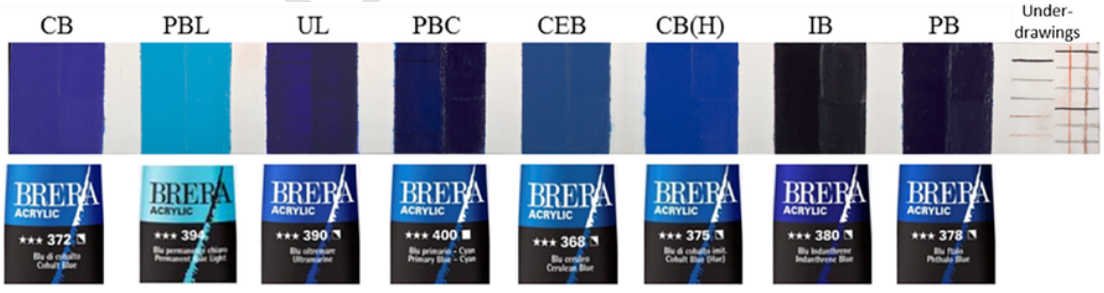

Fig. 2. Maimeri paint layers as applied on the wooden support with acrylic ground and underdrawings.

Table 1
Description of examined extrafine acrylic paints (Industria Maimeri spa, Brera Acrylic).

Pigments	Product codes	Commercial names	Abbreviation	Composition
Inorganics	0806368	Cobalt blue	CEB	Cobalt aluminium oxides - PB
	0806372	Ultramarine	UL	Sodium polysulphide - allumir PB29 – 77007
	0806390	Cerulean blue	CB	Cobalt aluminium-chromium (PB36 – 77343
Organics	0806400	Primary blue – cyan	PBC	Phthalocyanine β - PB15:3 – 7
	0806380	Indanthrene blue	IB	6,15-Dihydro-5,9,14,18-anthra ($C_{28}H_{14}N_2O_4$) PB60 – 69800
	0806378	Phthalo blue	PB	Phthalocyanine α - PB15:1 – 7
Mixtures	0806375	Cobalt blue (Hue)	CB(H)	Sodium polysulphide -allumin PB29 - 7707 Phthalocyanine β - PB15:3 - ' Titanium dioxide - PW6 – 77
	0806394	Permanent blue light	PBL	Chlorinated phthalocyanine - I phthalocyanine beta - PB15:3 Titanium dioxide - PW6 – 77

tracted to obtain the paint thicknesses and to yield information on paint homogeneity by formation of false colour 3D maps.

2.2.2. Optical coherence tomography

The home-build instrument is a time-domain set-up, operating with sensitivity of about 75 dB and at 4 Hz in A-scan. The device is associated with a confocal microscope optics, which allows for a lateral resolution down to 2.5 μm. The spectral width ($\Delta\lambda$ = 100 nm) of the light source centred at λ = 1550 nm sets the axial resolution to about 10 μm in air. The working distance of the objective lens from the surface is about 3 mm. The simplified scheme of the device is shown in Fig. 3.

B-scan (cross-sectional image) of the paint, acquired by translating the probing beam along a 10 mm line, is presented in this paper. The axial (depth) scale in the OCT cross-sectional image is elongated compared to the lateral one. The apparent optical distances in OCT tomogram need to be divided by index of refraction in order to obtain the real distances. The 5 × 5 × 1 mm^3 OCT tomocubes were acquired with 25 μm lateral sampling step. The OCT tomocubes were elaborated with Image J software. First, proper slicing with a plane parallel to the preparatory layer was computed. The signal maxima were then projected point-by-point to obtain well-contrasted image of the preparatory layer with underdrawing. 50–100 slices starting from the preparation layer were considered for the former projection.

2.2.3. Vis-NIR scanning reflectography

The instrument used for multispectral imaging is a scanning device [26], providing a set of images (16 in the Vis and 16 in the NIR range) that can be analysed either as a stack of wavelength-resolved images (multispectral Vis-NIR reflectography) or as a series of point reflectance spectra, one for each sampled pixel on the surface (Vis-NIR spectrometry). The spectral range covered by the instrument is 400–2500 nm, with spectral resolution 20–30 nm and 50–100 nm in the Vis and NIR spectral region, respectively. The spatial sampling is

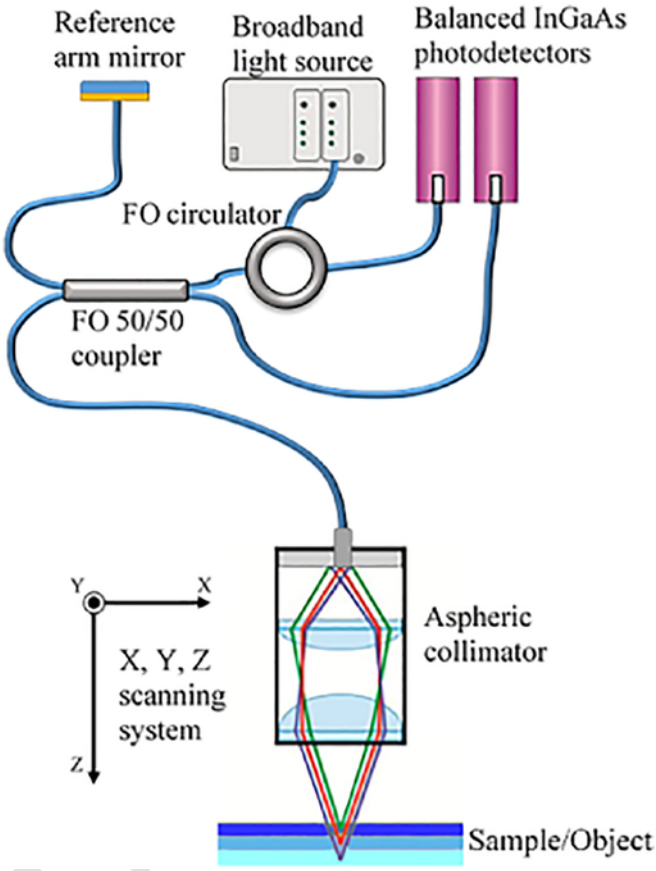

Fig. 3. Simplified scheme of time-domain OCT prototype (FO – fiber optics).

250 μm and the acquisition speed is 3 h per square meter. In spite that all the 16 NIR reflectograms were recorded, only the one in the 1450–1550 nm spectral window is shown in this article in order to match it as closely as possible with the working spectral range of OCT (λ = 1550 nm, $\Delta\lambda$ = 100 nm). Moreover, the high-resolution reflectance spectra of the paints were obtained with commercial spectrometers (Zeiss MCS 521 VIS-NIR-E and MCS-511 NIR 1.7), having the density of spectral sampling equal to 3 and 6 nm, respectively.

3. Results

The experiment was designed to examine paints containing 3 inorganic (Ultramarine (*UL*), Cobalt (*CB*) and Cerulean (*CEB*) blues), 3 organic (Phthalocyanines alfa (*P-α*) and beta (*P-β*), and Indanthrene blue (*IB*)) paints and 2 mixtures. The two inspected mixtures are a combination of the previously mentioned pigments/dyes: 1) ultramarine and *P-β,* and 2) chlorinated phthalo and *P-β*. These two mixtures were chosen for the presence of TiO_2 pigment.

3.1. Microprofilometric investigation of paint thicknesses

As a first step, the real thickness of the applied paints was calculated as the height differences of the two conoscopic measurements. The first acquisition was performed on the bare preparation layer (ground level) with the paper tape (reference level) used for delimiting the areas of single paints (t_0) and the second one (t_1), performed on painted samples of thicknesses I, II, and III. Data were processed in Matlab environment to yield false colour maps of thickness values generated by subtraction of these two measurements $z(t_1)$-$z(t_0)$. As

determined by laser microprofilometry, the paint layers present thicknesses of approximately 100, 200 and 300 μm. An example of the false colour 3D map of phthalo paint is reported in Fig. 4, along with the extracted height profiles across two different thicknesses.

3.2. Underdrawing visibility examined by OCT and VIS-NIR scanning reflectography

For all the samples, the OCT profiles (B-scans), across different thicknesses, were acquired. An example of a 10 mm long B scan acquired on Phthalo blue paint is shown in Fig. 5. The paint represents low-scattering medium located between the top air/paint interface and the paint/ground on the bottom.

To verify the visibility of underdrawing, 5 × 5 × 1 mm^3 tomocubes were systematically acquired with lateral steps of 25 μm on all the samples starting from the lowest thickness paint. The most significant results are shown in Figs. 5–9 and can be summarized as follows. The tin/lead trait was detected under *PB* (phthalo α), *PBC* (phthalo β), *IB*, and *UL* for all the paint thicknesses (100–300 μm); under *CB*, *CB*(*H*) and *PBL* for the first thickness (100 μm). On the other hand, no underdrawing was revealed under *CEB* paint.

As a part of the designed experiment, the specimens were examined also with VIS-NIR scanner. To make any useful comparison with OCT (excitation wavelength centred at 1550 nm) results, the reflectograms centred at 1500 nm were analysed. In specific, the sepia, lead/tin and charcoal traits were detected in the 1450–1550 nm reflectograms under all the paints but the cobalt-based ones (*CB* and *CEB*). The results obtained by both techniques are summarized in Table 2.

3.2.1. Underdrawings detectable with both imaging modalities

Both reflectography and OCT proved effective in the detection of underdrawing in most blue paints, namely Phtalo, Ultramarine, Primary Cyan, Ultramarine, Cerulean Hue, and Permanent Light.

PB is discussed firstly as an example of transparent paint, as probed by both NIR reflectography and OCT. RGB image (Fig. 6a) and 1500 nm NIR reflectogram (Fig. 6b) of the 3 × 2.5 cm^2 painted zone and OCT tomocube (Fig. 6c) are shown. Different underdrawing sketches are evident in the reflectogram, thus proving the paint's transparency at 1500 nm. The OCT tomocube and the relative image of signal maxima projection ((Fig. 6d) clearly evidence the feasibility to image the Pb/Sn trait on the preparatory layer. The corresponding behaviour was observed in *UL, PBC* and *IB* paints. This result is in line with those published by Szkulmowska et al. [18], stating good transparency of ultramarine pigment.

The RGB image of *CB*(*H*) paint and 1500 nm reflectogram are shown respectively in Figs. 7a and b. The paint's transparency at 1.5 μm is evidenced by the visibility of the underdrawing in the reflectogram. The tin/lead stylus was detected by OCT only under the 100 μm thick paint, as reported in Figs. 7c and e. At higher paint thickness, the graphic trait was not revealed (Fig. 7d and f). It is worth to consider that *CB*(*H*) is a mixture of synthetic ultramarine, phthalocyanine β and titanium dioxide. The first two components, investigated as single paints (*UL* and *PBC*), prove transparent in OCT. Therefore, it can be hypothesized that the limits in the detection of the underdrawing are due to the scattering properties of TiO_2, masking the signal coming from the inner subsurface microstructure. The same applies to the second *PBL* mixture (chlorinated phthalo, phthalo β and TiO_2).

3.2.2. Underdrawing not detected by both imaging modalities

Only one paint proved opaque as examined by both methods, namely Cerulean blue paint (Fig. 8a). In specific, no graphic sketches are revealed underneath the paint by VIS-NIR imaging (Fig. 8b) and only the air/paint interface is evident in acquired OCT tomocube (Fig. 8c). Moreover, the depth averaged image in the plain of the paint sample (excluding the top interface) and the signal maxima projection did not allowed for the visualization of the traits on the substrate (Fig. 8d). This can be explained by the strong absorption band of *CEB* pigment in the 1.2–1.55 μm zone due the ligand-field-transition in the d-d orbitals of the ion Co (II) [27]. The absorption of the radiation is the main factor influencing the limited possibility to probe the inner structure of the Co-based paints.

3.2.3. Underdrawing visible only when probed by OCT

The detection of the underdrawing was achieved with OCT, but not with reflectography, only in the case of Cobalt blue (Fig. 9a). As shown in the 1450–1550 nm reflectogram (Fig. 9b), the graphic traits cannot be visualized through any of the paint thicknesses. This is primarily due to the strong absorption of the incoming radiation by the paint and, subsequently, to the insufficient contrast between the underdrawings and the preparatory layer - i.e. the difference between the absorbed and reflected components. On the other hand, the OCT reached the limit of detection at 100 μm thick paint (graphic trait detected – Fig. 9c and e). At higher *CB*(*H*) paint thicknesses no graphic pattern was discerned (Fig. 9d and f).

As a complementary results, the reflectance spectra between 1500 and 1600 nm are shown in Fig. 10 for all the paints. The absorbing paints (Co-based) exhibit very low reflectance values (< 4%), whereas the transparent paints collocate in the 50–65%R range and the mixtures above 70%R.

The two cobalt blue pigments exhibit a typical absorption band in the infrared region (around 1200–1500/1600 nm), due to the elec-

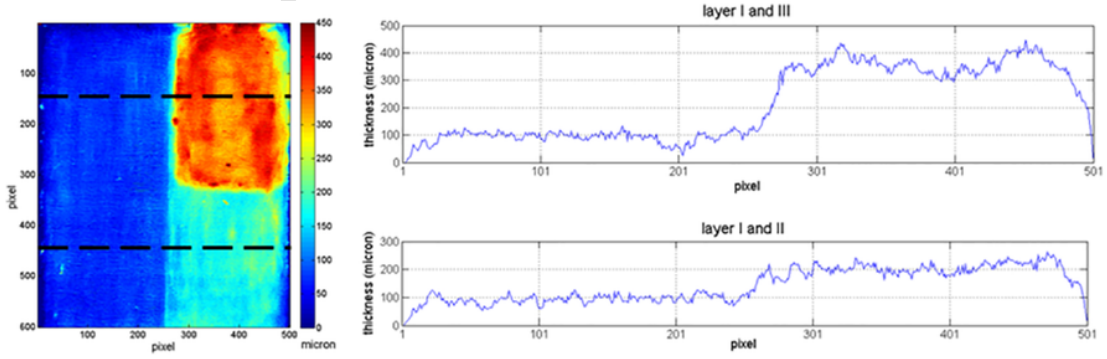

Fig. 4. False colour 3D map (left) of height differences of the phthalo paint and extracted height profiles (right) across different thickness (black dashed lines). 1 pixel corresponds to 50 μm.

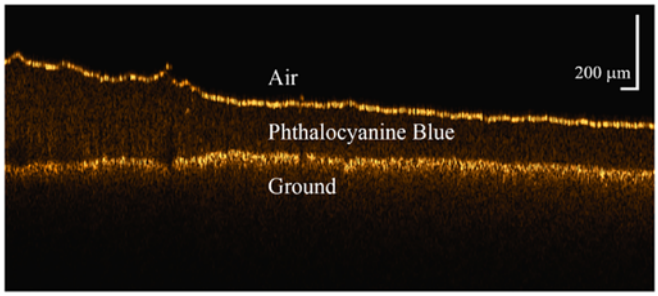

Fig. 5. Phthalo blue (PB): OCT B-scan of across two thicknesses. (For interpretation of the references to colour in this figure legend, the reader is referred to the web version of this article.)

tronic transitions in crystalline lattice, in specific among the *d* orbitals of cobalt ions. The slightly lower reflectance values were detected for the Cerulean blue paint in comparison with Cobalt blue, in agreement with the partial transparency observed by OCT in the latter. This study confirms that the presence of TiO_2 in acrylic paints affects the detectability of underdrawing patterns realized on acrylic preparation layers. Also Cheung et al. [21] demonstrated high turbidity of titanium white at 930 nm, 1310 nm and its transparency at 1960 nm.

4. Conclusion

The paper presents a background work describing some of the optical properties of modern acrylic blue paints. Information concerning the visibility of graphic traits under paint layers is crucial in view of minimising invasive physical sampling. The response of contemporary blue paints was examined by VIS-NIR reflectography and OCT, complemented with other methods, as a function of paint thickness. The results clearly show the effectiveness of both methods in visualizing the graphic traits under the synthetic organic paints - both polymorphs of Phthalocyanine blue (α and β), Indanthrene (anthracene derivative), as well as the ultramarine paints. The obtained results promote the application of OCT in probing contemporary paintings, in which synthetic organic paints and dyestuffs are often the main constituents. The phthalocyanine blues, first introduced commercially in the 1930s, represent the most widely used class of these pigments. Some limits in revealing the underdrawing were encountered when probing the Cobalt (detected under 100 μm thick paint) and Cerulean blues, as well as on the mixed paints containing titanium dioxide.

Acknowledgments

The research leading to the prototype of confocal microscope was funded by the EU Community's FP7 Research Infrastructures

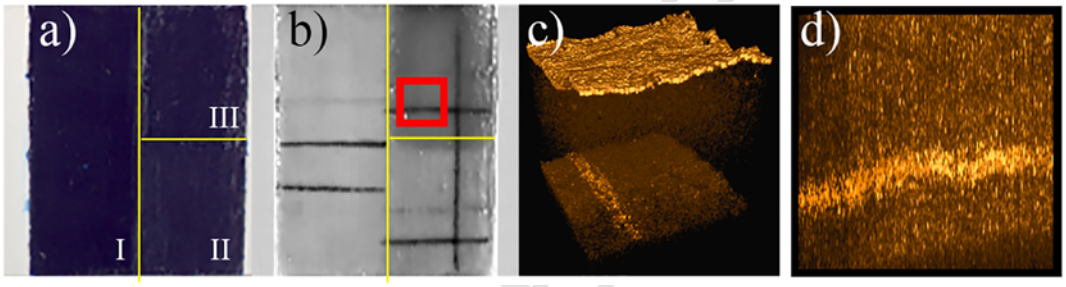

Fig. 6. Phthalo blue paint: a) RGB image, b) NIR reflectogram at 1500 nm and c) 5 × 5 × 1 mm^3 OCT tomocube (the image is stretched in z direction for better visualization), d) resliced tomocube with projection of signal maxima in z direction in the plane of the preparation layer. The red box in b) designates the position of the tomocube acquired on the 300 μm thick paint. (For interpretation of the references to colour in this figure legend, the reader is referred to the web version of this article.)

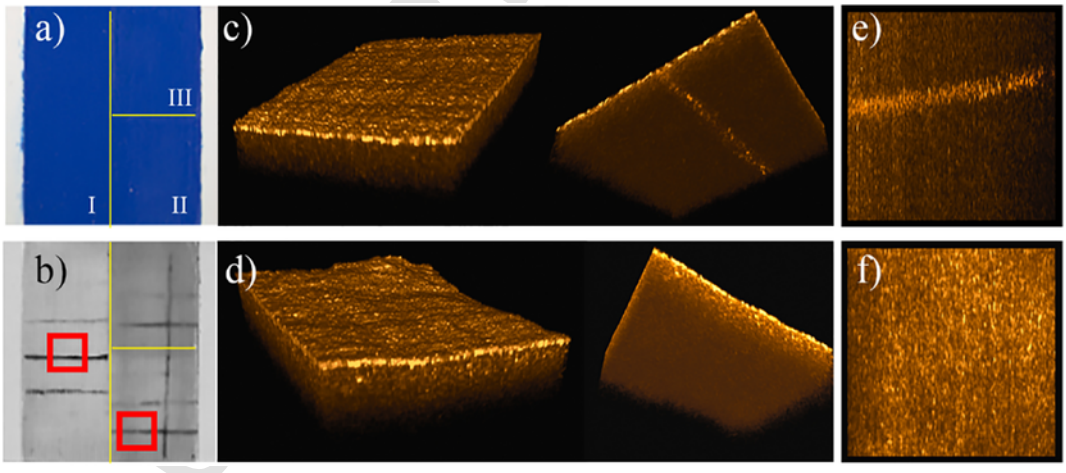

Fig. 7. CB(H) paint: a) RGB image, b) NIR reflectogram at 1500 nm, c) and d) 5 × 5 × 1 mm^3 OCT tomocubes (the image is stretched in z direction for better visualization), e) and f) resliced tomocubes with projection of signal maxima in z direction in the plane of the preparation layer. The red boxes in b) designate the position of the tomocubes acquired on the 100 and 200 μm thick paint shown in c) and d), respectively. (For interpretation of the references to colour in this figure legend, the reader is referred to the web version of this article.)

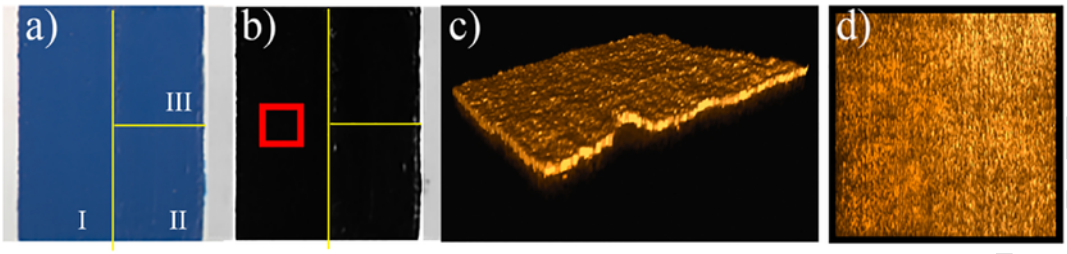

Fig. 8. Cerulean blue paint: a) RGB image, b) NIR reflectogram at 1500 nm, c) 5 × 5 × 1 mm^3 OCT tomocube (the image is stretched in z direction for better visualization), d) resliced tomocube with projection of signal maxima in z direction in the plane of the preparation layer. The red box in b) designates the position of the tomocube acquired on the 100 μm thick paint. (For interpretation of the references to colour in this figure legend, the reader is referred to the web version of this article.)

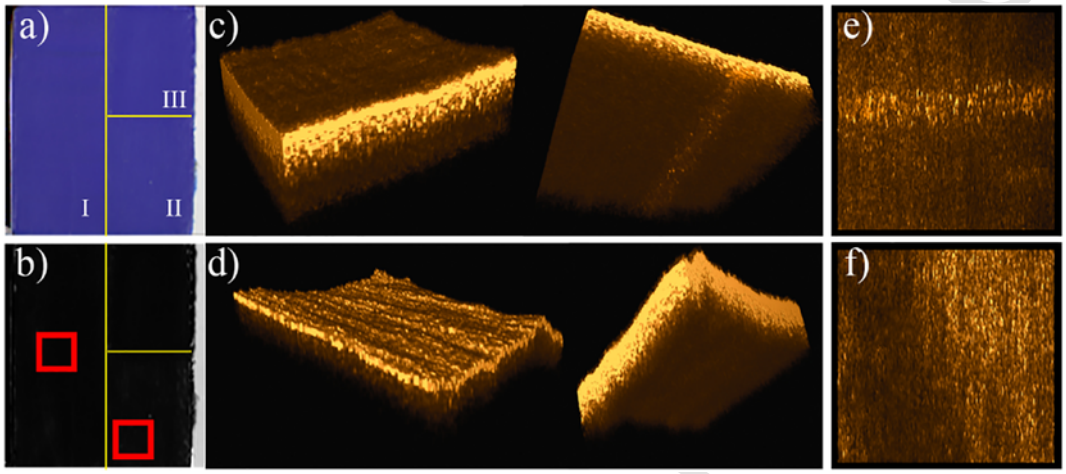

Fig. 9. Cobalt blue paint: a) RGB image, b) NIR reflectogram at 1500 nm, c) and d) 5 × 5 × 1 mm^3 OCT tomocube (the image is stretched in z direction for better visualization), e) and f) resliced tomocubes with projection of signal maxima in z direction in the plane of the preparation layer. The red boxes in b) designate the position of the tomocubes acquired on the 100 and 200 μm thick paint shown in respectively c) and d). (For interpretation of the references to colour in this figure legend, the reader is referred to the web version of this article.)

Table 2
Paint layers examined by OCT and VIS-NIR scanner. *Partial* refers to 100 μm thickness, *Yes* up to 300 μm.

Pigments	Abbreviation	Composition	Visibility of OCT at 1550 nm (1500–1600
Inorganics	*CEB*	Cobalt aluminium-chromium oxides	*No*
	CB	Cobalt aluminium oxides	*Partial*
	UL	Sodium polysulphide – alluminosilicate	*Yes*
Organics	*PBC*	Phthalocyanine β - PB15:3	*Yes*
	IB	6,15-Dihydro-5,9,14,18-anthrazinetetrone	*Yes*
	PB	Phthalocyanine α - PB15:1	*Yes*
Mixtures	*CB*(*H*)	Sodium polysulphide -alluminosilicate phthalocyanine β - PB15:3, TiO_2	*Partial*
	PBL	Chlorinated phthalocyanine phthalocyanine β- PB15:3, TiO_2	*Partial*

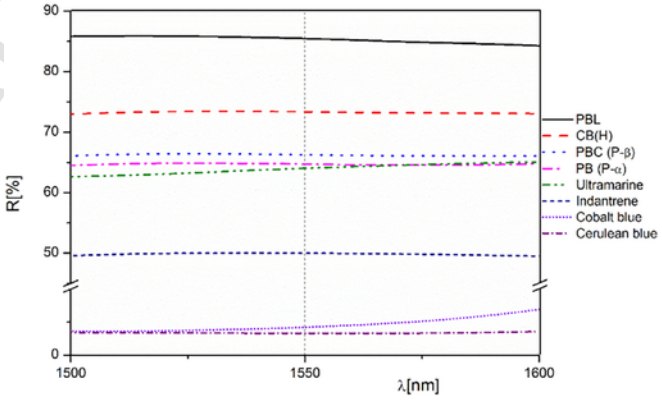

Fig. 10. Reflectance spectra of examined paints (first thickness) in the 1500–1600 nm range.

Programme under the CHARISMA Project (GA 228330). In the framework of the project, the instrument was modified and transformed in a confocal OCT device. The research leading to these results was funded by the EU Community's H2020 Research Infrastructure program under the IPERION CH Project (GA 654028).

References

[1] D. Huang, E.A. Swanson, C.P. Lin, J.S. Schuman, W.G. Stinson, W. Chang, M.R. Hee, T. Flotte, K. Gregory, C.A. Puliafito, J.G. Fujimoto, Optical coherence tomography, Science 254 (1991) 1178–1181.

[2] A.F. Fercher, W. Drexler, C.K. Hitzenberger, T. Lasser, Optical coherence tomography—principles and applications, Rep. Prog. Phys. 66 (2003) 239–303.

[3] P.H. Tomlins, R.K. Wang, Theory, developments and applications of optical coherence tomography, J. Phys. D 38 (2005) 2519–2535.

[4] W. Drexler, J.G. Fujimoto, Optical Coherence Tomography Technology and Applications, 2nd edition, Springer International Publishing, Switzerland, 2015, (ISBN 978-3-319-06419-2).

[5] References at http://www.oct4art.eu: Optical Coherence Tomography For Examination of Works of Art (accessed 1/4/2017).

[6] M.L. Yang, C.W. Lu, I.J. Hsu, C.C. Yang, The use of optical coherence tomography for monitoring the subsurface morphologies of archaic jades, Archaeometry 46 (2004) 171–182.

[7] P. Targowski, B. Rouba, M. Wojtkowski, A. Kowalczyk, The application of optical coherence tomography to nondestructive examination of museum objects, Stud. Conserv. 49 (2) (2004) 107–114.

[8] H. Liang, M.G. Cid, R.G. Cucu, G.M. Dobre, A.Gh. Podoleanu, J. Pedro, D. Saunders, En-face optical coherence tomography – a novel application of non-invasive imaging to art conservation, Opt. Express 13 (2005) 6133–6144.

[9] T. Arecchi, M. Bellini, C. Corsi, R. Fontana, M. Materazzi, L. Pezzati, A. Tortora, Opt. Spectrosc. 101 (2006) 23, https://doi.org/10.1134/S0030400X06070058.

[10] P. Targowski, M. Iwanicka, L. Tyminska-Widmer, M. Sylwestrzak, E.A. Kwiatkowska, Structural examination of easel paintings with optical coherence tomography, Acc. Chem. Res. 43 (2010) 826–836.

[11] P. Targowski, M. Iwanicka, Optical coherence tomography: its role in the non-invasive structural examination and conservation of cultural heritage objects—a review, Appl. Phys. A Mater. Sci. Process. 106 (2012) 265–277.

[12] S. Lawman, H. Liang, High precision dynamic multi-interface profilometry with optical coherence tomography, Appl. Opt. 50 (32) (2011) 6039.

[13] J. Striova, R. Fontana, M. Barucci, A. Felici, E. Marconi, E. Pampaloni, M. Raffaelli, C. Riminesi, Optical devices provide unprecedented insights into the laser cleaning of calcium oxalate layers, Microchem. J. 124 (2016) 331–337.

[14] P. Targowski, J. Marczak, E.A. Kwiatkowska, M. Sylwestrzak, A. Sarzyński, Optical coherence tomography for high-resolution real-time varnish ablation monitoring, in: D. Saunders, M. Strlič, C. Korenberg, N. Luxford, K. Birkhölzer (Eds.), Lasers in the Conservation of Artworks IX (Proceedings of Lacoana IX conference), London, UK, September 7–10, 2011, Archetype Publications Ltd, London, 2013, pp. 26–31.

[15] M. Iwanicka, G. Lanterna, C.G. Lalli, F. Innocenti, M. Sylwestrzak, P. Targowski, On the application of optical coherence tomography as a complimentary tool in an analysis of the 13th century byzantine Bessarion reliquary, Microchem. J. 125 (2016) 75–84.

[16] R. Fontana, A. Dal Fovo, J. Striova, L. Pezzati, E. Pampaloni, M. Raffaelli, M. Barucci, Application of noninvasive optical monitoring methodologies to follow and record painting cleaning processes, Appl. Phys. A Mater. Sci. Process. 121 (3) (2015) 957–966.

[17] J. Striova, B. Salvadori, R. Fontana, A. Sansonetti, M. Barucci, E. Pampaloni, E. Marconi, L. Pezzati, M.P. Colombini, Optical and spectroscopic tools evaluating Er:YAG laser removal of shellac varnish, Stud. Conserv. 60 (2015) S91–96.

[18] H. Liang, R. Lange, B. Peric, M. Spring, Optimum spectral window for imaging of art with optical coherence tomography, Appl. Phys. B Lasers Opt. 111 (4) (2013) 589–602.

[19] A. Szkulmowska, M. Góra, M. Targowska, B. Rouba, D. Stifter, E. Breuer, P. Targowski, The applicability of optical coherence tomography at 1.55 μm to the examination of oil paintings, In: LACONA VI Proceedings, Vienna, Austria, Sept. 21–25, Vol. 116, 2005, pp. 487–492, Springer Proceedings in Physics.

[20] H. Liang, B. Peric, M. Hughes, A.G. Podoleanu, M. Spring, S. Roehrs, Optical coherence tomography in archaeological and conservation science - a new emerging field, Proc. SPIE 7139 (2008), 713915.

[21] H. Liang, B. Peric, M. Spring, D. Saunders, M. Hughes, A.Gh. Podoleanu, Non-invasive imaging of subsur paint layers with optical coherence tomography, in: Joyce Townsend, et al. (Eds.), Conservation Science 2007, Milan, 10–11 May 2007, Archetype publishing, London, 2008, pp. 171–176.

[22] C.S. Cheung, M. Spring, H. Liang, Ultra-high resolution Fourier domain optical coherence tomography for old master paintings, Opt. Express 23 (8) (2015) 10145–10157, https://doi.org/10.1364/OE.23.010145.

[23] C.S. Cheung, J.M.O. Daniel, M. Tokurakawa, W.A. Clarkson, H. Liang, High resolution Fourier domain optical coherence tomography in the 2 μm wavelength range using a broadband supercontinuum source, Opt. Express 23 (2015) https://doi.org/10.1364/OE.23.001992.

[24] C.S. Cheung, J.M.O. Daniel, M. Tokurakawa, W.A. Clarkson, H. Liang, Optical coherence tomography in the 2-μm wavelength regime for paint and other high opacity materials, Opt. Lett. 39 (22) (2014) 6509–6512.

[25] C. Conti, M. Realini, C. Colombo, A. Botteon, M. Bertasa, J. Striova, M. Barucci, P. Matousek, Determination of thickness of thin turbid painted over-layers using micro-scale spatially offset Raman spectroscopy, Phil. Trans. R. Soc. A 22 (2016) 1055–1060, https://doi.org/10.1098/rsta.2016.0049.

[26] R. Fontana, M. Barucci, E. Pampaloni, J. Striova, L. Pezzati, From Leonardo to Raffaello: Insights by VIS-IR Reflectography Presented in: 5th ALMA interdisciplinary Conference: Interpretation of Fine Art's Analyses in Diverse Contexts, Academy of Fine Arts in Prague, 20145–16, (ISBN: 978-80-87108-48-2).

[27] M. Bacci, D. Magrini, M. Picollo, M. Vervat, A study of the blue colors used by Telemaco Signorini (1835–1901), J. Cult. Herit. 10 (2009), (275–28).